ARTICLE

Composite Cathode based on Mn-doped Perovskite Niobate-Titanate for Efficient Steam Electrolysis

Jun Zhang[a], Kui Xie[a,b*], Yuan-xin Li[a], Wen-tao Qi[a], Cong Ruan[a], Yu-cheng Wu[a,b*]

a. Department of Energy Materials, School of Materials Science and Engineering, Hefei University of Technology, Hefei 230009, China
b. Key Laboratory of Advanced Functional Materials and Devices, Hefei University of Technology, Hefei 230009, China

(Dated: Received on March 28, 2014; Accepted on May 8, 2014)

Redox-active Mn is introduced into the B site of redox-stable perovskite niobate-titanate to improve the electrocatalytic activity of composite cathode in an oxide-ion-conducting solid oxide electrolyzer. The XRD and XPS results reveal the successful partial replacement of Ti/Nb by Mn in the B site of niobate-titanate. The ionic conductivities of the Mn-doped niobate-titanate are significantly improved by approximately 1 order of magnitude in reducing atmosphere and 0.5 order of magnitude in oxidizing atmosphere compared with bare niobate-titanate at 800 °C. The current efficiency for Mn-doped niobate-titanate cathode is accordingly enhanced by ∼25% and 30% in contrast to the bare cathode with and without reducing gas flowing over the cathode under the applied voltage of 2.0 V at 800 °C in an oxide-ion-conducting solid oxide electrolyzer, respectively.

Key words: Perovskite, Ionic conductivity, High temperature steam electrolysis, Oxide-ion-conducting, Solid oxide electrolyzer

I. INTRODUCTION

Solid oxide electrolyzers have attracted a lot of interest because they can directly and efficiently convert renewable electrical energy into chemical fuel energy [1, 2]. Steam electrolysis is regarded as an efficient method in producing hydrogen owing to the favourable thermodynamics and kinetics at elevated temperatures [3]. Under a certain external applied voltage, H_2O molecules are electrochemically reduced into H_2 in the cathode and O^{2-} ions are simultaneously transported through the oxide-ion-conducting electrolyte to the anode where pure oxygen is formed and released [4, 5].

Traditional composite cathode material Ni/YSZ is widely used for high-temperature steam electrolysis in the solid oxide electrolyzer and exhibits good performances under reducing condition [6]. However, Ni metal can be easily oxidized into NiO if the direct steam electrolysis is performed with the composite cathode [7]. It has been reported that a significant concentration of reducing gas was required to flow over the electrode otherwise the Ni would be easily oxidized by leading to the loss of electrical conductivity, degradation of electrode performance and even the delamination of the electrode from the electrolyte surface [8].

Compared with Ni/YSZ, perovskite-type LSCM ($La_xSr_{1-x}Cr_yMn_{1-y}O_{3-\delta}$) has been proven an active and redox stable material which can be used as both cathode and anode in high temperature solid oxide fuel cell [9]. Recently, Irvine *et al.* reported that direct steam electrolysis based on the ceramic cathode LSCM without the flow of reducing gas over the composite electrode and the results showed that the composite cathode was stable without any performance degradation in the electrolysis [10]. However, insufficient catalytic activity of LSCM cathode limits the electrolysis performances as reported in our previous report [11]. On the other hand, some chemical and structural changes occurring in the LSCM cathode under strong reducing potentials also degrade the electrode performances [11]. The perovskite-type ($La_xSr_{1-x}TiO_{3-\delta}$) LSTO is also an active and redox-stable material which has high n-type electronic conductivity in reduced state [12]. The metallic behavior of the electronic conductivity well adapts to the strong reducing atmosphere of the cathode under electrolysis conditions. Nevertheless, the insufficient catalytic activity still limits the electrode polarization and current efficiency for the high temperature electrolysis. It was found that the current efficient of H_2O electrolysis based on LSTO composite cathode was 70%−75%, the result was so low [13].

Currently, more and more attention has been paid to the niobate-titanate doping into the B site, where Nb^{5+} substitutes Ti^{4+}, which has significantly improved the electrochemical properties [14]. According to a previous report, the electrical conductivity of $Sr_{0.9}Ti_{0.8}Nb_{0.2}O_3$

*Authors to whom correspondence should be addressed. E-mail: xiekui@hfut.edu.cn

reached a high level (approximately 340 S/cm) at 800 °C in reducing atmosphere [15]. Chen and his coworkers have researched the influence of Ga-doped A site deficient $Sr_{0.9}Ti_{0.8}Nb_{0.2}O_3$ and found that the sample with 10%Ga doping demonstrated the highest electrical conductivity in reducing atmosphere at high temperature [16]. In addition, it was also indicated the excellent redox stability of $SrNb_xTi_{1-x}O_3$ materials after the oxidizing and reducing treatments in air or wet H_2 at elevated temperatures [17]. Hence, composite cathode based on niobate-titanate would adapt to the reducing condition for the electrolysis of steam in an oxide-ion conducting solid oxide electrolyzer. The niobate-titanate solid solution can be partially electrochemically reduced ($Ti^{4+}\rightarrow Ti^{3+}$ and $Nb^{5+}\rightarrow Nb^{4+}$) under applied potentials and the active Ti^{3+} and Nb^{4+} would act as a catalytic-active site to further improve the cathode performances with favourable kinetics in addition to the significant improvement of electronic conductivity because of the high concentration of Ti^{3+} and Nb^{4+} in the B site.

In this work, the redox-active Mn is doped to $Sr_{0.95}Ti_{0.9}Nb_{0.1}O_3$ (STNO) to enhance the electrode performances and elevate the current efficiency of the electrode for the high temperature steam electrolysis. The electrical properties including electronic conductivity, oxide-ion conductivity and n-type metallic behavior are investigated. Direct electrolysis of steam with the cathode based on the Mn-doped STNO is then performed with or without the flow of reducing gas over the cathode in an oxide-ion conducting solid oxide electrolyzer, respectively.

II. EXPERIMENTS

All the chemicals (99.9%) were purchased from Sinopharm Chemical Reagent Co. Ltd. (China). The $Sr_{0.95}Ti_{0.8}Nb_{0.1}Mn_{0.1}O_3$ (STNMO) powders were synthesized by the traditional solid state reaction method. Stoichiometric amounts of $SrCO_3$, TiO_2, Nb_2O_5, and MnO_2 powders were mixed together and ball milled for 15 min in acetone; then the dried powders were pressed into pellets and fired at 1300 °C for 10 h in air [18]. The powders of $Sr_{0.95}Ti_{0.9}Nb_{0.1}O_3$ (STNO) were prepared as the way above. The $(La_{0.8}Sr_{0.2})_{0.95}MnO_{3-\delta}$ (LSMO) were synthesized using the above method by mixing the proper amounts of La_2O_3, $SrCO_3$ and MnO_2 and the heat treatment temperature was 1100 °C for 10 h in air [19]. The $Ce_{0.8}Sm_{0.2}O_{2-\delta}$ (SDC) powders were prepared by the combustion method in which the Sm_2O_3 and $Ce(NO_3)_3{\cdot}6H_2O$ powders were mixed and sintered at 800 °C for 3 h in air [20]. The phase formation of the STNMO, STNO, LSMO and SDC powders were all analyzed by X-ray diffraction (XRD, 2θ=3°/min, D/MAX2500V, Rigaku Corporation, Japan). In addition, X-ray photoelectron spectroscopy (XPS) was performed on a Thermo ESCALAB 250 to analyze the surface of the oxidized and reduced STNMO and STNO sample powders, the binding energies were calibrated to the C1s peak at 284.6 eV.

About 2.5 g STNMO and STNO powders were pressed into bars and sintered at 1300 °C for 10 h in air for the conductivity test. The relative density of the sintered disks reached approximately 80%−85%. Before the conductivity test of reduced samples, the bars of STNMO and STNO were reduced at 1400 °C for 10 h in 5%H_2/Ar, respectively. The DC four-terminal method was used for the conductivity test in the reducing atmosphere (5%H_2/Ar). The temperature ranged from 30 °C to 800 °C with a step of 3 °C/min while the conductivity was recorded with an online system at a time step of 10 s. The conductivity was recorded versus temperature from 30 °C to 800 °C at the beginning and then versus the oxygen partial pressure (p_{O_2}) from 10^{-20} atm to 10^{-2} atm using a mass flow meter while the conductivity was accordingly recorded at 800 °C. p_{O_2} and the conductivity were simultaneously recorded with an online oxygen sensor (Type 1231, ZrO_2-based oxygen sensor, Noveltech, Australia) and an online multi-meter (Keithley 2000, Digital Multimeter, Keithley Instruments Inc., USA), respectively. In addition, the ion conductivity of samples versus temperature from 400 °C to 800 °C were tested by the electronic blocking method in oxidized and reduced situation, respectively [21, 22].

The YSZ electrolyte support with thickness of 1 mm was made by dry-pressing the YSZ powders into a green disk with a diameter of approximate 15 mm, followed with a sintering at 1550 °C for 20 h in air. The two surfaces of the electrolyte were mechanically polished and ultrasonically washed in the ethanol and distilled water. The slurry of cathode STNMO/SDC or STNO/SDC was prepared by milling STNMO or STNO powders with SDC powders at a weight ratio of 65:35 in α-terpineol with the appropriate amount of cellulose additive [23, 24]. The LSMO and SDC powders were also mixed together at a weight ratio of 65:35 in α-terpineol with the appropriate amount of cellulose additive to prepare the anode slurry. Then, the two kinds of slurry were coated onto the two sides of the electrolyte in the area of approximately 1 cm^2 and the sample was sintered at 1000 °C for 3 h in air. The current collector of silver paste (SS-8060, Xinluyi, Shanghai, China) was printed on both surfaces of the electrodes. The silver wire (0.4 mm in diameter) was used to form the circuit by conductive adhesive (DAD87, Shanghai Research Institute for Synthetic Resins, Shanghai, China), and treated at 550 °C for 0.5 h in air. The electrolysis cells were sealed to a homemade testing jig using ceramic paste (JD-767, Jiudian, Dongguan, China) for electrochemical test. The steam electrolysis in the solid oxide electrolyzer based on the STNMO/SDC and STNO/SDC cathode was tested under different applied voltages at 800 °C in 3%H_2O/5%H_2/Ar and 3%H_2O/Ar, respectively. The

DOI:10.1063/1674-0068/27/04/457-464

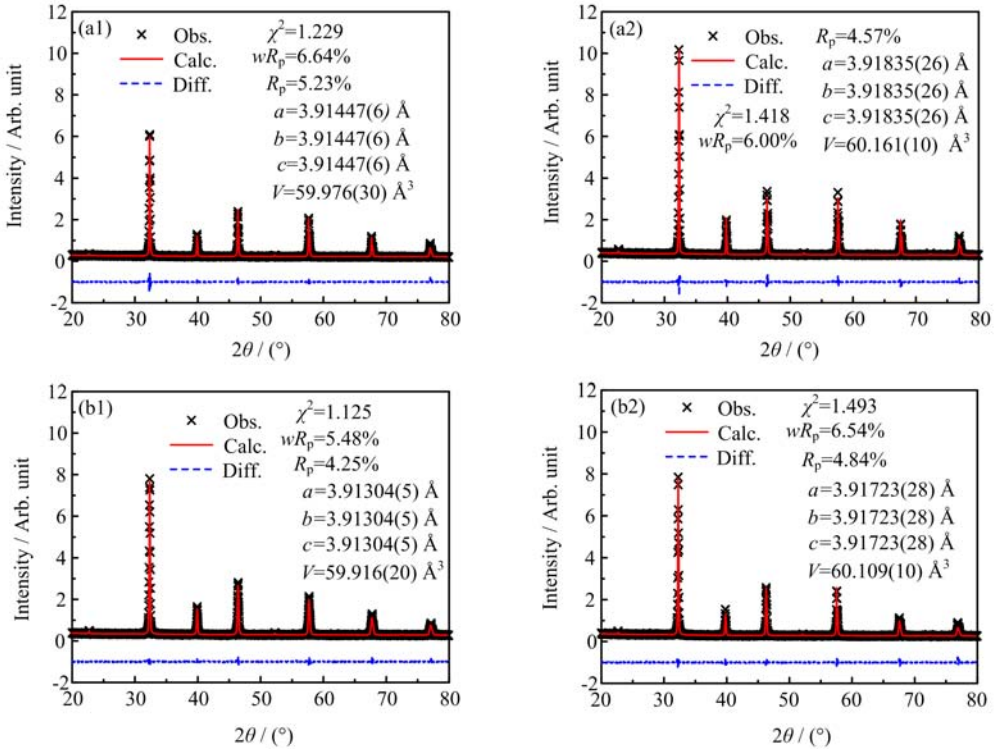

FIG. 1 XRD patterns of (a) STNO and (b) STNMO in the oxidized (left panel) and reduced state (right panel).

in situ AC impedance spectroscopy and the current density versus voltage curve (I-V curve) of the electrolysis cell were recorded by the Electrochemical Station (IM6, Zahner, Germany). The online gas chromatograph (GC9790II, Fuli, Zhejiang, China) was used to analyze the H_2 concentration of the output gas from the electrolyzer cells.

III. RESULTS AND DISCUSSION

Figure 1(a) shows the XRD Rietveld refinement patterns of the oxidized and reduced STNO powders, respectively. The refinement of the oxidized and reduced samples give the χ^2 (fitting factor), wR_p (weighting surplus factor)) and R_p (surplus factor) values of 1.229, 6.64%, 5.23% and 1.418, 6.00%, 4.57%, respectively, indicating a close fit to the experimental data. Based on experimental and calculated results, it indicates that phase structure of both oxidized and reduced samples can be determined as perovskite structure with space group of $Pm3m$ [25]. The crystal cell parameter of the oxidized STNO is 3.91447(6) Å which is slightly smaller than that of the reduced STNO, 3.91835(26) Å. The chemical oxidation states of the Ti and Nb are +4 with ionic radii of 0.605 Å and +5 with 0.64 Å in the oxidized STNO, respectively. In contrast, parts of the Ti and Nb have been transformed into Ti^{3+} (0.67 Å) and Nb^{4+} (0.68 Å) the reduced STNO sample which may cause the lattice expansion through the oxygen loss is present after high-temperature reduction. Nevertheless, no phase transition is observed in the STNO even after the high-temperature treatment in a reducing atmosphere, firmly verifying superior redox stability of the niobate-titanate ceramics. In Fig.1(b), XRD Rietveld refinement patterns of single-phase STNMO reveal the successful partial replacement of Ti by Mn in the B site. The refinement of the oxidized and reduced samples give χ^2, wR_p and R_p values of 1.125, 5.48% and 4.25% as well as 1.493, 6.54% and 4.84%, respectively. The cell parameter is 3.91304(5) Å for the oxidized STNMO smaller than that of the oxidized STNO sample, which is because of the smaller ionic radius of the Mn^{4+} (0.53 Å) in contrast to the Ti^{4+} and Nb^{5+}. However, the cell parameter of the reduced STNMO is increased to 3.91723(28) Å because of the partial transformation of the Mn^{4+}, Nb^{5+}, and Ti^{4+} into Mn^{3+} (0.645 Å), Nb^{4+} (0.68 Å), and Ti^{3+} (0.67 Å) leading to the expansion of the cell parameters of the reduced samples.

To confirm the elemental valence change, XPS analysis is performed to test the oxidized and reduced STNMO samples. As shown in Fig.2, the strong signal of the Ti^{4+} and Nb^{5+} is observed in the oxidized sample; however, part of the Ti^{4+} and Nb^{5+} are chemically reduced to Ti^{3+} and Nb^{4+} by treating the samples in reducing atmosphere as confirmed by the signal of Ti^{3+} and Nb^{4+} which is expected to significantly contribute to the electronic conductivity. The Mn^{4+} ($2p_{1/2}$) and

DOI:10.1063/1674-0068/27/04/457-464

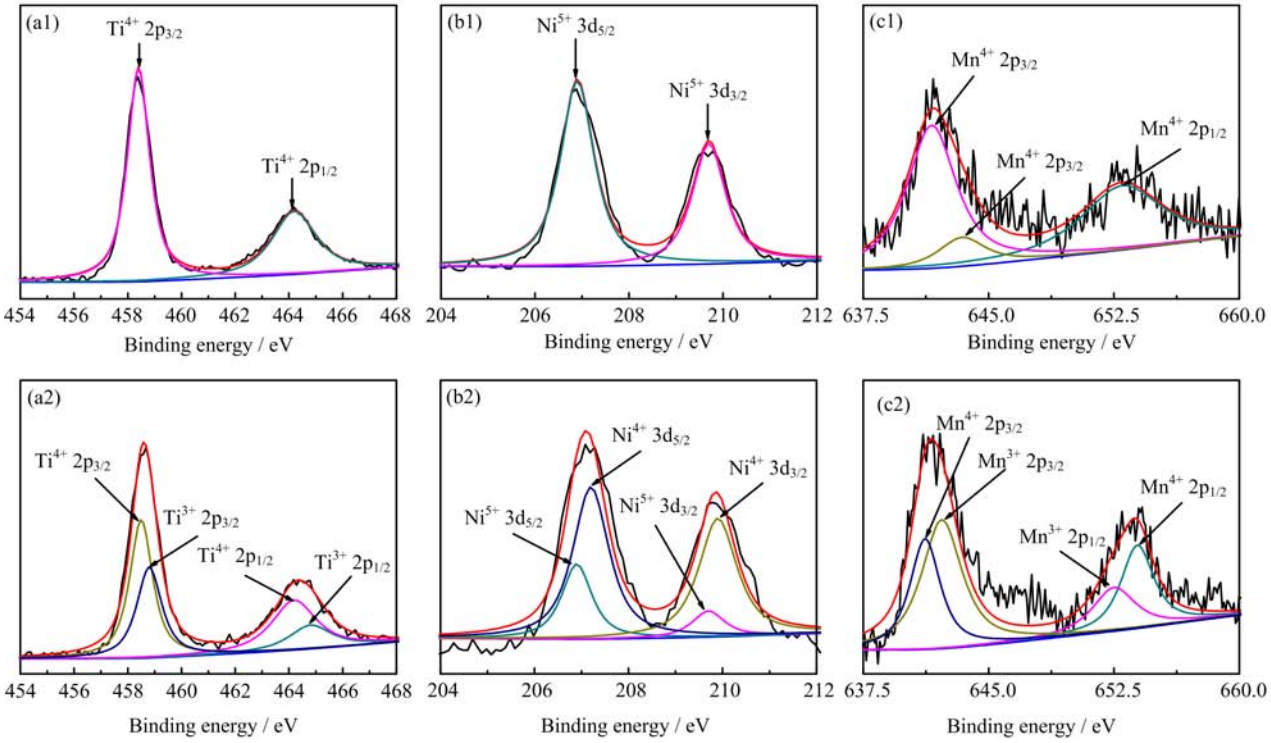

FIG. 2 XPS results of STNMO. (a) Ti, (b) Ni, (c) Mn in the oxidized (upper panel) and reduced state (lower panel).

Mn^{4+} ($2p_{3/2}$) peaks are observed at 653.90, 643.4, and 640.4 eV in Fig.2(c1), indicating the redox activity of the Mn element in the sample. The XPS data further reveal that Mn^{4+} is chemically reduced to Mn^{3+} by treating the STNMO samples in reducing atmosphere which is expected to create the oxygen vacancies and the concentration of the oxygen vacancy is strongly related to the amount of the low-valence ions in B site.

The dependence of conductivity on temperature and p_{O_2} is carried out to investigate the electrical properties of STNO and STNMO samples, respectively. The conductivity of the reduced STNO and STNMO samples displays typical metallic behaviors with negative temperature coefficients in 5%H_2/Ar, indicating the typical n-type conducting mechanism in reducing atmospheres. As shown in Fig.3(a), the reduced STNMO and STNO demonstrate similar conductivity values in 5%H_2/Ar and finally reach approximately 15.8 and 25 S/cm, respectively. The conductivity of the reduced STNO is higher than that of the reduced STNMO which is probably due to Mn doping in B site of STNMO and therefore the consumption of electron with hole generated by the combination of oxygen vacancy and atmospheric oxygen. The adsorption of oxygen would oxidize Ti^{3+} to Ti^{4+} and Nb^{4+} to Nb^{5+} on the surface of reduced STNO and STNMO, which produced an oxidized and p-type conducting samples layer on the surface and caused the low conductivity at low temperatures. It is also observed that the conductivity of the reduced STNO and STNMO samples are strongly dependent on p_{O_2} as shown in Fig.3(b). The n-type conductivity rapidly decreases as the p_{O_2} rises in the range of 10^{-16}–10^{-15} atm, which is due to the transition of Ti^{3+} to Ti^{4+} in the gradually decreased reducing atmosphere at 800 °C. However, the conductivity is stable in a wide

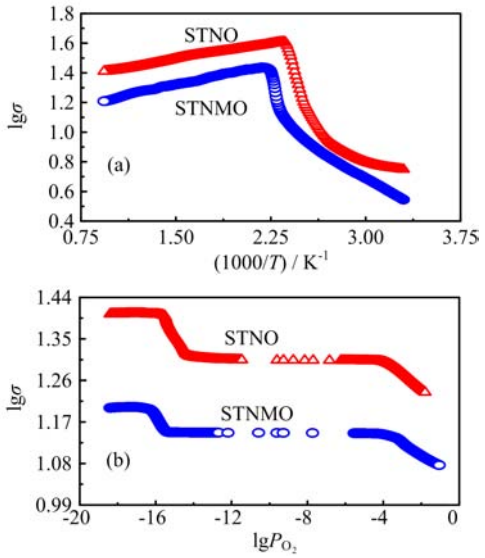

FIG. 3 The conductivities of STNO and STNMO as functions of (a) temperature (from 30 °C to 800 °C) in the flow of 5%H_2/Ar gas, and (b) oxygen partial pressure (from about 10^{-20} atm to 10^{-2} atm).

DOI:10.1063/1674-0068/27/04/457-464

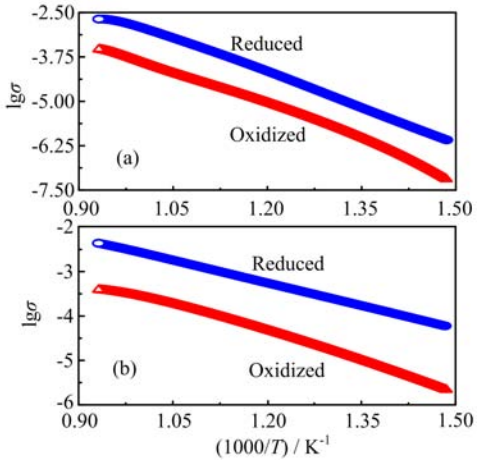

FIG. 4 The ion conductivity of samples in oxidized and reduced situations, respectively. (a) STNO, (b) STNMO.

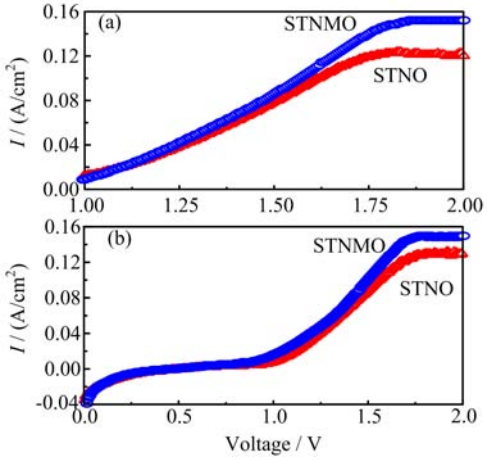

FIG. 5 The *I-V* curves of two kinds of electrolysis cells at 800 °C in different atmosphere conditions. (a) 3%H_2O/5%H_2/Ar, (b) 3%H_2O/Ar.

range of p_{O_2} which is probably due to the rapid change of p_{O_2} in this range and the sample may be not at the equilibrium state that causes the inconsistent change of conductivity. In addition, the significant decrease of the conductivity is observed with the p_{O_2} above 10^{-4} atm due to the sufficient oxidization of Ti^{3+} to Ti^{4+} in the samples and the sample would finally transform to a p-type conductor with pretty low conductivity at 800 °C in air. With the formation of oxygen vacancy in the samples, the ionic conductivity of Mn-doped niobate-titanate is expected to be remarkably improved.

Figure 4(a) shows the temperature dependence of ionic conductivity of the oxidized and reduced STNO in air and 5%H_2/Ar from 400 °C to 800 °C, respectively. The ionic conductivities of the oxidized and reduced STNO are also improved with temperature and finally reach 1.7×10^{-4} and 1.9×10^{-3} S/cm in air and 5%H_2/Ar at 800 °C, respectively. It is apparent that the reduced sample with high concentration of oxygen vacancy strongly benefits the ionic conductivity. In Fig.4(b), the ionic conductivities of the oxidized and reduced STNMO reach 3.16×10^{-4} and 3.98×10^{-3} S/cm in air and 5%H_2/Ar at 800 °C, respectively. The introduction of redox-active Mn significantly enhances the ionic conductivity of STNMO compared to the STNO because of the creation of charge carrier, oxygen vacancy, in the sample. However, the oxidized STNMO has low ionic conductivities though it is higher than the oxidized STNO sample, which is probably attributed to the insufficient oxygen vacancy as the charge carrier for the oxide ion transport in sample. Upon reduction, the STNMO with high concentration of oxygen vacancy shows the significantly improved oxide-ion conductivity by 1 order of magnitude higher in reducing atmosphere at intermediate temperatures.

Figure 5 shows the current density with applied voltage (*I-V* curve) of two kinds of electrolyzers under different testing conditions. The relationships between the current density and applied voltage are far from linear and clear changes in slope can be observed at approximately 1.2 V. As shown in Fig.5(a), the maximum current density reaches 152.4 mA/cm^2 at 2.0 V based on the STNMO/SDC composite cathode, while the current density only reaches 121.3 mA/cm^2 with the bare STNO/SDC electrode in 3%H_2O/5%H_2/Ar, which indicates that the doped Mn significantly enhances the cell performance for the direct steam electrolysis. Similar behavior was also observed for the electrolyzers in the 3%H_2O/Ar as shown in Fig.5(b), where the current density reaches 156.1 mA/cm^2 at 2.0 V with STNMO/SDC composite cathode; however, only 123 mA/cm^2 is achieved with the STNO/SDC composite cathode, which further confirms the improvement of electrode performance with the doped Mn even in a less reducing atmosphere (3%H_2O/Ar).

In Fig.6 (a) and (b), the current densities versus time under different applied voltage (1.2, 1.4, 1.6, 1.8 and 2.0 V) are tested to further study the processes of steam electrolysis. The current densities increase with the applied voltage and the performance was stable at a certain voltage load. It can be found that the current densities reaches 119.5 mA/cm^2 at 2.0 V with the STNMO/SDC composite electrodes which is higher than 109.6 mA/cm^2 at 2.0 V for the bare STNO/SDC composite electrodes in the 3%H_2O/5%H_2/Ar, further indicating the improved performances of the electrode with the doped Mn. In addition, the current density with the STNMO/SDC cathode reaches 140.2 mA/cm^2 at 2.0 V for the direct steam electrolysis in 3%H_2O/Ar which is also higher than that of the bare STNO/SDC cathode 122.7 mA/cm^2. To further study the electrochemical performance of the electrodes, *in situ* AC impedance spectroscopy is carried out to investigate the change of cell resistance under different voltage.

Figure 7 exhibits the *in situ* AC impendence of

DOI:10.1063/1674-0068/27/04/457-464

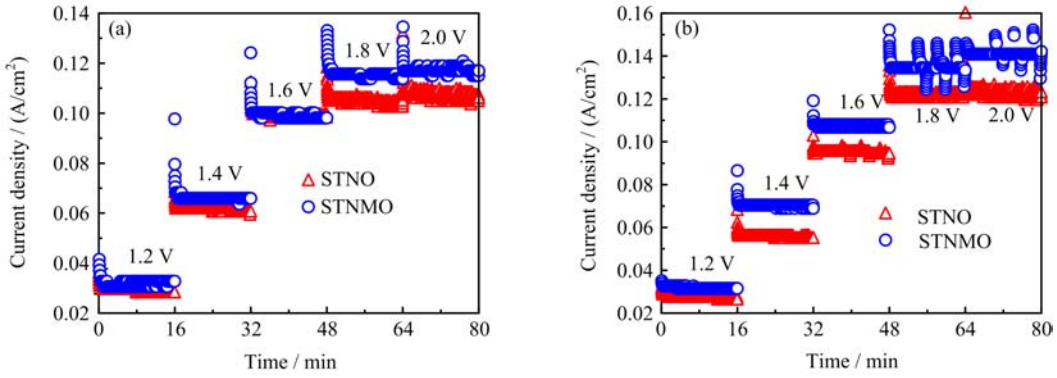

FIG. 6 The performances of steam electrolysis for two kinds of electrolysis cells in different atmosphere conditions at 800 °C. (a) 3%H_2O/5%H_2/Ar, (b) 3%H_2O/Ar.

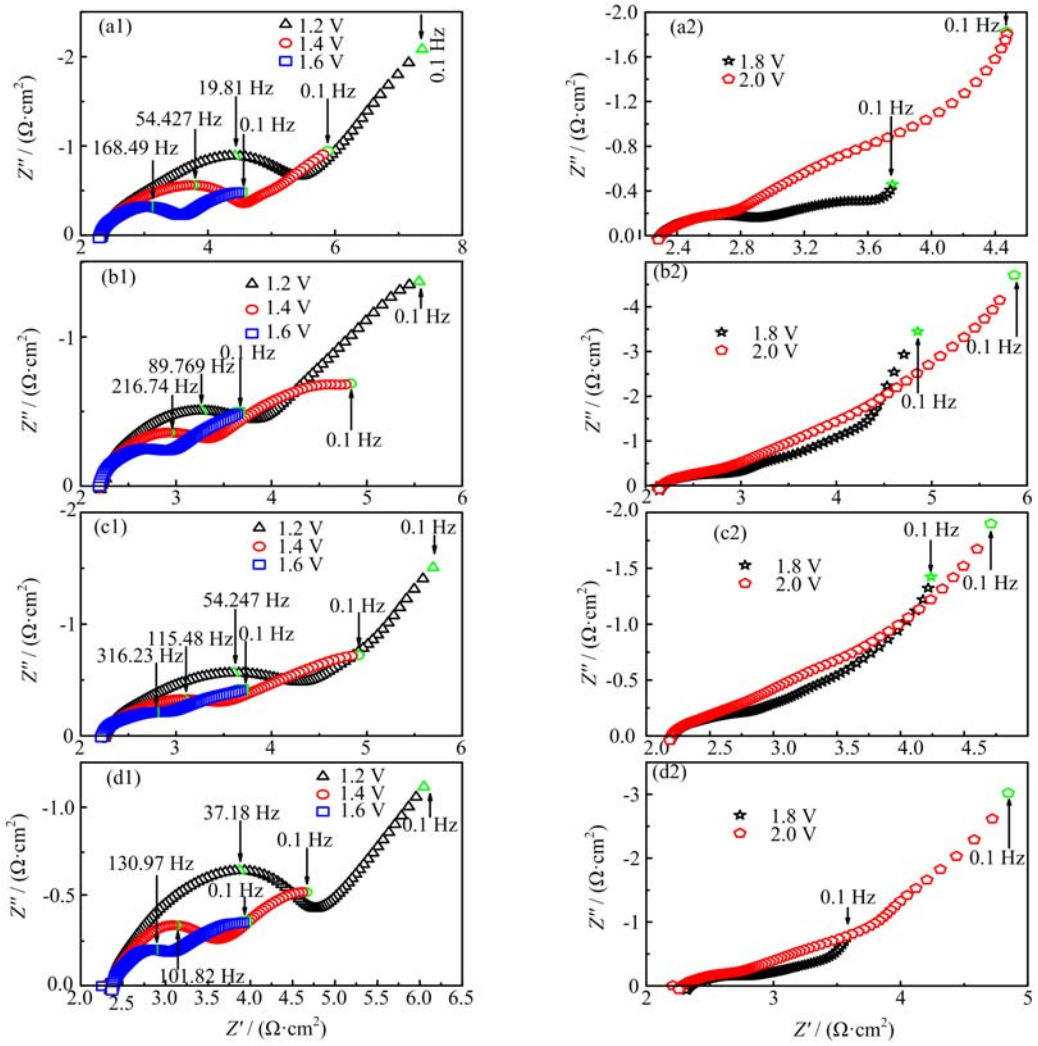

FIG. 7 The *in situ* AC impendence of the electrolysis cells based on STNO/SDC (a1, a2) and STNMO/SDC (b1, b2), with the flow of 3%H_2O/5%H_2/Ar and different applied voltage at 800 °C. The AC impendence of the electrolysis cells based on STNO/SDC (c1, c2) and STNMO/SDC (d1, d2), with the flow of 3%H_2O/Ar and different applied voltage at 800 °C.

DOI:10.1063/1674-0068/27/04/457-464

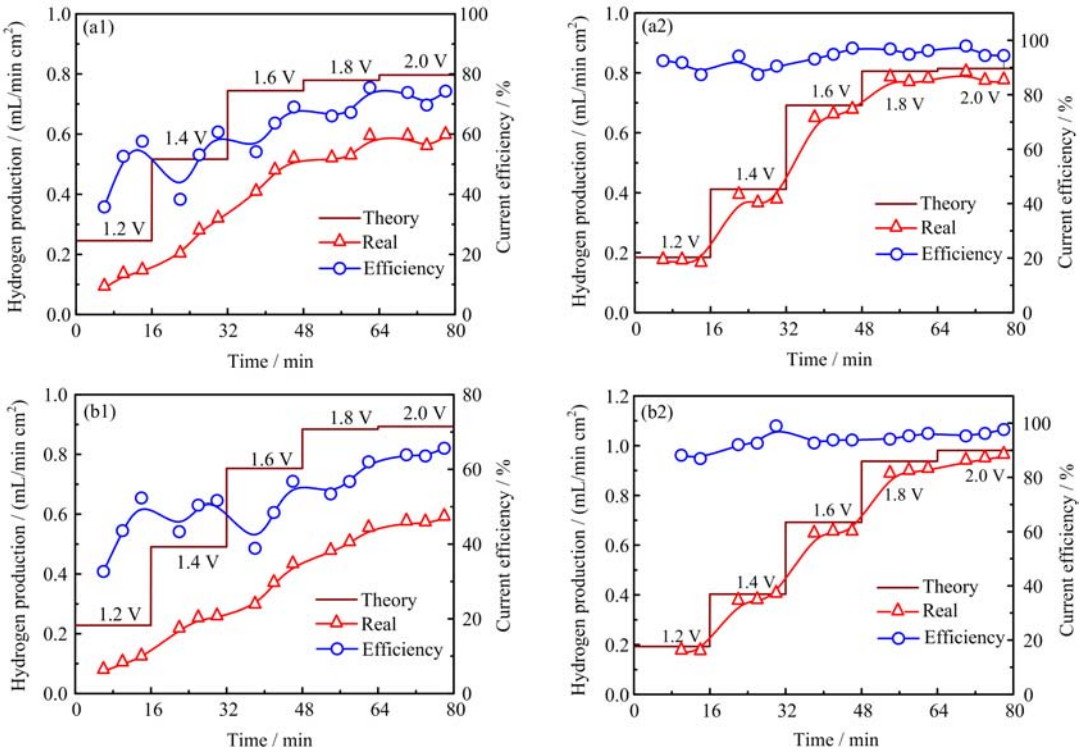

FIG. 8 The hydrogen production (theory and real value) and current efficiency for electrolysis cells. (a1) STNO and (a2) STNMO with the flow of 3%H_2O/5%H_2/Ar. (b1) STNO and (b2) STNMO with the flow of 3%H_2O/Ar.

solid oxide electrolyzers under a series of external voltages ranging from 1.2 V to 2.0 V at 800 °C in 3%H_2O/5%H_2/Ar and 3%H_2O/Ar, respectively. As shown in the figures, the electrode polarization resistance (R_p) seems quite large at low voltage while the increasing voltages make the R_p considerably drop at high voltages, indicating that the applied voltage not only activates the electrodes but also electrochemically reduces the composite electrode and enhances the mixed conductivity. The R_p is only 2.8 Ω·cm^2 at 1.6 V in 3%H_2O/5%H_2/Ar with STNMO/SDC composite cathode, while it is approximately 4.0 Ω·cm^2 at 1.6 V with STNO/SDC composite cathode as shown in Fig.7 (a1) and (b1). In Fig.7 (c) and (d), the electrochemical performance of the STNMO/SDC composite cathode is also evaluated in the atmosphere of 3%H_2O/Ar for the direct steam electrolysis. The electrode polarization resistance with the STNMO/SDC composite cathode is 2.7 Ω·cm^2 at 1.6 V and R_p of the bare STNO/SDC composite cathode is about 3.3 Ω·cm^2 at 1.6 V. Figure 7 also shows that R_p based on the STNO/SDC and the STNMO/SDC composite electrodes both strongly increase at the voltage higher than 1.8 V in two kinds of atmosphere while the current densities are not increased after applying approximately 1.8 V during the electrolysis as shown in Fig.5 (a) and (b), which is probably due to the local starvation of steam in the electrode at high current densities.

Figure 8 shows the rate of hydrogen production and the current efficiency of the electrolyzers based on the STNMO/SDC and the STNO/SDC composite cathodes for steam electrolysis at the different applied voltages in the atmospheres of 3%H_2O/5%H_2/Ar and 3%H_2O/Ar at 800 °C, respectively. The hydrogen production rate is calculated from the gas chromatograph results. The maximum hydrogen production for the cell based on the STNMO/SDC composite electrode, as shown in Fig.8(a2), is 0.8 mL/(min cm^2), which is higher than 0.6 mL/(min cm^2) at 2.0 V with the STNO/SDC composite electrode in the flow of 3%H_2O/5%H_2/Ar. Similarly, the maximum hydrogen production for the cell based on the STNMO/SDC composite electrode reaches 0.9 mL/(min cm^2), which is also higher than 0.6 mL/(min cm^2) for the STNO/SDC at 2.0 V without the reducing gas flowing over the cathodes. For the STNO/SDC cathode, the maximum current efficiencies reach 75% and 65% in the flow of 3%H_2O/5%H_2/Ar and 3%H_2O/Ar at 800 °C, respectively. In contrast, the maximum current efficiencies of the cell based on the STNMO/SDC cathode were elevated to 97% and 98% with and without the flow of reducing gas, respectively. Obviously, the solid oxide electrolyzer based on the STNMO/SDC cathode presented better performance than the STNO/SDC cathode, which is attributed to the doped Mn and the redox-stable ceramic STNO/SDC electrode.

Figure 9 shows the configuration of STNO/SDC-YSZ-LSMO/SDC and STNMO/SDC-YSZ-LSMO/SDC

DOI:10.1063/1674-0068/27/04/457-464

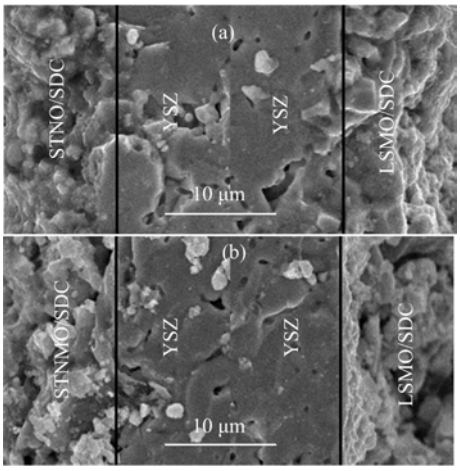

FIG. 9 The microstructure of electrolyzers with formation of (a) STNO/SDC-YSZ-LSMO/SDC and (b) STNMO/SDC-YSZ-LSMO/SDC.

for solid oxide electrolyzers, respectively. The YSZ electrolyte supports are quite uniform and dense with the porous electrode layers adhere to the electrolyte very well. The thicknesses of STNO and STNMO are 10 μm, respectively. In addition, both of them have similar porosity. No cracks or delaminations are observed after the steam electrolysis test, indicating better compatibility between the electrode and the electrolyte.

IV. CONCLUSION

In this work, the Mn-doped perovskite niobate-titanate has been investigated as a potential cathode material for high temperature steam electrolysis. It is observed that the high oxygen vacancy concentration caused by the Mn doping leads to robust enhancement of ionic conductivity and the electrode polarizations. The highest current efficiencies of 98% are obtained for the direct electrolysis of H_2O in addition to the promising electrode polarization based on Mn-doped cathode in an oxide-ion conducting solid oxide electrolyzer.

V. ACKNOWLEDGEMENTS

This work was supported by the National Natural Science Foundation of China (No.21303037), China Postdoctoral Science Foundation (No.2013M53150), and the Fundamental Research Funds for the Central Universities (No.2012HGZY0001).

[1] X. M. Ge, S. H. Chan, Q. L. Liu, and Q. Sun, Adv. Energy Mater. **2**, 1156 (2012).
[2] T. Ishihara, N. Jirathiwathanakul, and H. Zhong, Energy Environ. Sci. **3**, 665 (2013).
[3] M. A. Laguna-Bercero, R. Campana, A. Larrea, J. A. Kilner, and V. M. Orera, J. Power Sources **196**, 8942 (2011).
[4] M. Ni, M. K. H. Leung, and D. Y. C. Leung, Int. J. Hydrogen Energy **33**, 2337 (2008).
[5] G. Schiller, A. Ansar, M. Lang, and O. Patz, J. Appl. Electrochem. **39**, 293 (2009).
[6] C. Jin, C. H. Yang, and F. L. Chen, J. Electrochem. Soc. **158**, B1217 (2011).
[7] S. Lee, K. H. Kang, H. S. Hong, Y. S. Yun, and S. K. Woo, Int. J. Mater. Res. **99**, 114 (2008).
[8] Y. X. Li, J. E. Zhou, D. H. Dong, Y. Wang, J. Z. Jiang, H. F. Xiang, and K. Xie, Phys. Chem. Chem. Phys. **14**, 15547 (2012).
[9] W. Y. Tan, Q. Zhong, H. Yan, X. F. Zhu, and H. Y. Li, Int. J. Hydrogen Energy **37**, 7398 (2012).
[10] X. D. Yang and J. T. S. Irvine, J. Mater. Chem. **18**, 2349 (2008).
[11] Y. X. Li, Y. Gan, Y. Wang, K. Xie, and Y. C. Wu, Int. J. Hydrogen Energy **38**, 10196 (2013).
[12] S. S. Li, Y. X. Li, Y. Gan, K. Xie, and G. Y. Meng, J. Power Sources **218**, 244 (2012).
[13] Y. Gan, Q. Q. Qin, S. G. Chen, Y. Wang, D. H. Dong, K. Xie, and Y. C. Wu, J. Power Sources **245**, 235 (2014).
[14] J. T. S Irvine, P. R. Slater, and P. A. Wright, Ionics **2**, 213 (1996).
[15] T. Kolodiazhnyi and A. Petric, J. Electroceram. **15**, 5 (2005).
[16] G. L. Xiao, X. H. Dong, K. Huang, and F. L. Chen, Mater. Res. Bull. **46**, 57 (2011).
[17] P. Blennow, K. K. Hansen, L. R. Wallenberg, and M. Mogensen, Solid State Ionics **180**, 63 (2009).
[18] G. L. Xiao, S. Nuansaeng, L. Zhang, S. Suthirakun, A. Heyden, H. Z. Loye, and F. L. Chen, J. Mater. Chem. A **1**, 10546 (2013).
[19] H. P. He, Y. Y. Huang, J. Regal, M. Boaro, J. M. Vohs, and R. J. Gorte, J. Am. Ceram. Soc. **87**, 331 (2004).
[20] G. Jung and T. Huang, J. Mater. Sci. **38**, 2461 (2003).
[21] X. Li, H. L. Zhao, F. Gao, Z. M. Zhu, N. Chen, and W. Shen, Ionics **179**, 1588 (2008).
[22] A. Endo, M. Ihara, H. Komiyama, and K. Yamada, Solid State Ionics **86-88**, 1191 (1996).
[23] K. Xie, R. Q. Yan, Y. Z. Jiang, X. Q. Liu, and G. Y. Meng, J. Membrane. Sci. **325**, 6 (2008).
[24] S. L. Wang, B. Lin, K. Xie, Y. C. Dong, X. Q. Liu, and G. Y. Meng, J. Alloy Compd. **468**, 499 (2009).
[25] J. Karczewski, B. Riegel, M. Gazda, P. Jasinski, and B. Kusz, J. Electroceram. **24**, 326 (2010).

DOI:10.1063/1674-0068/27/04/457-464